Colloids and Surfaces B: Biointerfaces 195 (2020) 111240

Contents lists available at ScienceDirect

Colloids and Surfaces B: Biointerfaces

journal homepage: www.elsevier.com/locate/colsurfb

Fabrication of electrochemical biosensor composed of multi-functional DNA/rhodium nanoplate heterolayer for thyroxine detection in clinical sample

Sun Yong Park[a], Jinmyeong Kim[a], Gyeonghye Yim[b], Hongje Jang[b], Yeonju Lee[a], Soo Min Kim[a], Chulhwan Park[a], Min-Ho Lee[c,*], Taek Lee[a,*]

[a] Department of Chemical Engineering, Kwangwoon University, Wolgye-dong, Nowon-gu, Seoul, 01899, Republic of Korea
[b] Department of Chemistry, Kwangwoon University, Wolgye-dong, Nowon-gu, Seoul, 01899, Republic of Korea
[c] School of Integrative Engineering, Chung-Ang University, Heukseok-dong, Dongjak-gu, Seoul, 06910, Republic of Korea

ARTICLE INFO

Keywords:
Thyroxine
Multi-functional DNA
Porous rhodium nanoplates
Electrochemical biosensor

ABSTRACT

Thyroxine (T4) contains four iodine atoms and is a major thyroid hormone synthesized in the thyroid gland. Abnormal levels of T4 in the body cause various endocrine diseases. The present study describes the fabrication of an electrochemical biosensor composed of a multi-functional DNA structure/rhodium nanoplates heterolayer for precise detection of T4 concentration. A DNA 3-way junction (3WJ) structure was designed as a multi-functional bioprobe to perform several functions (including target detection, electrochemical signal reporting, and immobilization) simultaneously. Binding between T4 and the T4 DNA aptamer was confirmed through enzyme-linked aptamer assays (ELAAs) and filtration experiments. The multi-functional DNA was immobilized on porous rhodium nanoplates (pRhNPs)-heterolayer modified Au micro-gap electrode. The pRhNPs provided an increment in the surface area and amplification of the electrochemical signal. Cyclic voltammetry (CV) and electrochemical impedance spectroscopy (EIS) were used to detect T4. Under optimal conditions, the limit of detection of T4 was found to be 10.33 pM. Furthermore, up to 11.41 pM of T4 could be detected in clinical samples. This study demonstrates the possibility of label-free detection of the T4 with multi-functional DNA/pRhNPs heterolayer that can be applied to small molecule detection platform in the near future.

1. Introduction

The synthesis and secretion of thyroid hormones (THs) are regulated by thyrotropin-releasing hormone (TRH) secreted from the hypothalamus and thyroid stimulating hormone (TSH) secreted from the anterior pituitary gland. The two THs, triiodothyronine (T3) and thyroxine (T4), are synthesized and secreted by the thyroid gland and are composed of three and four iodine atoms, respectively. The hormone secreted from the gland is about 80 % T4 and 20 % T3. Due to its hydrophobicity, most of the T4 exists bound to TH-binding proteins such as the thyroxine-binding globulin (TBG) or albumin. Only 0.03 % of the T4 exists in the plasma as free-T4. Free-T4 elicits a biological response upon entering target cells [1,2]. The normal range of free-T4 in human serum is 0.89–1.79 ng/dL. Abnormal levels of TH in the body cause endocrinopathies such as hyperthyroidism and hypothyroidism. Furthermore, the association between thyroid diseases and depression has long been recognized and accepted. Although several studies have shown that patients with thyroid diseases are more prone to develop depressive symptoms and vice versa [3], the mechanisms underlying the interactions between thyroid dysfunction and depression remain to be elucidated. Because abnormal levels of TH are associated with not only endocrine diseases but also with depression, it is very important to monitor the level of T4 in the body.

For the detection of small molecule including T4, the conventional methods need long detection times, complicated detection steps, and special system requirement [4]. Optical methods based on fluorescent or radioactive labeling are mass-dependent, although they are useful. Small molecules such a T4 are too light to obtain a significant signal [5,6]. It is therefore necessary to fabricate a novel method that is both rapid and specific. Among them, the electrochemical detection methods have been proposed as an alternative, as they are cost-effective (as they use inexpensive reagents and equipment) and not dependent on the mass of the target [7,8]. Besides, miniaturization of the system is also simple since the electrochemical signal is generated directly by the

* Corresponding authors.
E-mail addresses: mhlee7@cau.ac.kr (M.-H. Lee), tlee@kw.ac.kr (T. Lee).

https://doi.org/10.1016/j.colsurfb.2020.111240
Received 20 May 2020; Received in revised form 30 June 2020; Accepted 1 July 2020
Available online 02 July 2020

reaction of the target and probe.

In the meantime, the metal-DNA complexes consist of double-strands DNA (dsDNA) bound to metal ions [9–11]. Compared to free DNA, metal-DNA is more resistant to pH changes and is a better electrochemical signal reporter [12]. Copper (Cu^{2+}), mercury (Hg^{2+}), and silver (Ag^{+}) ions are representative metal ions capable of intercalating into the base pairs of DNA [13,14]. Especially, C-Ag^{+}-C (cytosine-silver ion-cytosine) mismatched dsDNA has structural, thermodynamic, and kinetic stability that can be easily applied to electrochemical biosensor [12].

The detection of T4 has been conventionally carried out using immunoassays. However, the antibody-based T4 detection method involves complex steps that has hampered its use for patients and researchers. The multi-functional DNA with a T4 DNA aptamer containing intercalated silver ions fabricated in this study resolves these problems. This system is based on porous rhodium nanoplates (pRhNPs) which facilitated the electrochemical signaling and provided surface roughness increment [15]. The pRhNPs were introduced to fabricate the electrochemical biosensor, for the first time. Electrochemical analysis was conducted using cyclic voltammetry (CV) and electrochemical impedance spectroscopy (EIS) methods. The EIS method specifically measures not only the electrochemical signal resulting from the reaction of T4 and probe, but also the changes of the electrode surface. It is therefore suitable for the development of label-free sensor because of its high sensitivity. Fig. 1 shows a schematic diagram of the fabricated biosensor system.

2. Experimental details

2.1. Materials

Hydrochloric acid and acetone were provided from Duksan Fine Chemicals (South Korea). CNBr-activated sepharose™ 4B was purchased from GE Healthcare (USA). L-thyroxine, streptavidin-Cy3, cysteamine, potassium hexacyanoferrate(III) and potassium hexacyanoferrate(II) trihydrate ($[Fe(CN)_6]^{3-/4-}$) were all purchased from Sigma-Aldrich (USA). The porous rhodium nanoplates (pRhNPs) were synthesized by following method [15]. Tris(hydroxymethyl)aminomethane, magnesium chloride, sodium chloride, sodium hydrogen carbonate, potassium chloride, ethylene glycol, ethyl alcohol, silver nitrate ($AgNO_3$) and 4-(2-Hydroxyethyl)piperazine-1-ethanesulfonic acid (HEPES) were all purchased from Daejung Chemical and Metals Co. Ltd. (South Korea). Dyne loadingSTAR from Dynebio Inc. (South Korea) was used to stain DNA at electrophoresis. The clinical samples of T4, this study protocol and pre-informed consent procedures were approved by the Institutional Review Board and the research ethics committees of Ewon Laboratories (IRB no. 128477-201, 611-ER-010). All subjects were informed by the investigator about the aims, methods, and potential hazards in this study.

All DNA were synthesized by Integrated Device Technology, Inc. (USA). The DNA sequences used were depicted as follows.

Biotinylated T4 DNA aptamer: 5`-Bio-TAA TAC GAC TCA CTA TAG GGA ATT CGT CGA CGG ATC CGC CGT TGG TGT TCG GTC AGG CTT CCG TGG CAA CGG GGC AAA ATG GTA ATC GCG GGG AAC CCT GCA GGT CGA CGC ATG CGC CG-3` [16]

Biotin-tagged control DNA: 5`-Bio-GGA TCA ATC ATG GCA A-3`

3WJ-a: 5`-TAA TAC GAC TCA CTA TAG GGA ATT CGT CGA CGG ATC CGC CGT TGG TGT TCG GTC AGG CTT CCG TGG CAA CGG GGC AAA ATG GTA ATC GCG GGG AAC CCT GCA GGT CGA CGC ATG CGC CGT TGC CAT GTG TAT GTG GG-3`

3WJ-b: 5`-TTC ACC CCT GAC ATG GCA A-3`

3WJ-c: 5`-SH-CCC ACA TAC CAC CCC TGA A-3`

2.2. Enzyme-linked aptamer assays (ELAAs) used T4 and T4 DNA aptamer

A total of 100 μl of 3 mM T4 solution containing 50 % (w/v) ethylene glycol and 500 mM $NaHCO_3$ (pH 9.6) was aliquoted into a 96-well plate and the plate was incubated for 24 h at 4 °C. Then the plate was inverted to drain out the solution. The T4 adsorbed on the plate was treated with 100 μl of 1 μM biotinylated T4 DNA aptamer (in 10 mM Tris, 1 mM $MgCl_2$, pH 7.6) for 4 h at room temperature. The biotinylated T4 DNA aptamer was heated before use for 5 min at 80 °C, followed by gradual cooling down to 4 °C in a T100™ thermal cycler (Bio-Rad, USA). The same procedure was repeated with biotin-tagged control DNA. The plates were washed once between each step with 300 μl of 0.05 % PBST solution and 100 μl of 1 μM streptavidin-Cy3 was added to each well of the plate. After incubation for 1 h at room temperature, the plates were rinsed with 300 μl of 0.05 % PBST solution. Then, 100 μl of PBS was added to each well, and the fluorescence intensity of samples in each well was measured at 540–600 nm (green filter) using a Synergy™ LX multi-mode microplate reader (BioTek, USA).

2.3. Filtration of sepharose-DNA-Cy3 complex

A total of 20 mg of CNBr-activated sepharose was suspended in 1.5 ml of 1 mM HCl for 1 h at 4 °C and dried. After the swelling process, 0.6 ml of 3 mM T4 was added to the sepharose beads and the mixture was rotated overnight at 4 °C [17,18]. Half of the T4-sepharose was reacted with 100 μl of 1 μM biotinylated T4 DNA aptamer and biotin-tagged control DNA for 2 h at room temperature, respectively. Each solution was mixed with 100 μl of 1 μM streptavidin-Cy3 solution for 1 h at

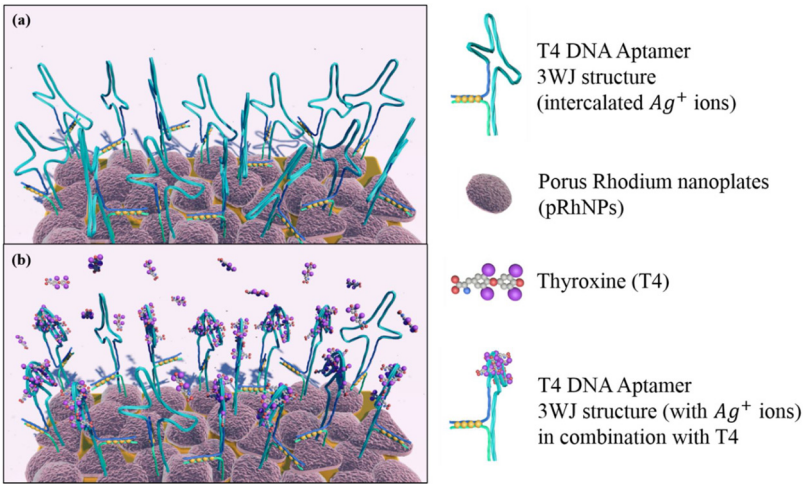

Fig. 1. Schematic diagram of the fabricated thyroxine (T4) detection biosensor (a) in conditions of T4 absence and (b) in conditions of T4 presence.

room temperature and then centrifuged at 3000 *g* for 20 min with 50,000 MWCO centrifugal filter (Merck Millipore, USA). The fluorescence intensity of each recovery was read on a microplate reader.

2.4. Assembly of the multi-functional DNA 3WJ (3-way junction) structure

Three different single-stranded DNA (ssDNA) of the corresponding sequences were introduced (3WJ-a, 3WJ-b, and 3WJ-c). 3WJ-a was composed of the T4 DNA aptamer for target detection [16]. A thiol-modified DNA was selected for the immobilization part of 3WJ-c. C-C (cytosine-cytosine) mismatches were used in the 3WJ-b and 3WJ-c portion. These ssDNA sequences were chemically synthesized. A silver ion was intercalated between C-C mismatched sequence for signal reporting of the electrochemical measurement [12,19]. The DNA 3WJ structure was assembled by annealing the three complementary strands of DNA at equal molar ratio in TMS buffer (50 mM Tris, 10 mM $MgCl_2$, 100 mM NaCl) by heating for 5 min at 80 °C, followed by cooling to 4 °C at a rate of 2 °C/min. Assembly of the DNA 3WJ structure was confirmed using tris-boric acid-magnessium-native polyacrylamide gel electrophoresis (8% TBM- PAGE). 100 bp DNA ladder from Bioneer Inc. (South Korea) was used to compare to DNA. About 0.02 nmol of DNA samples were electrophoresed at 70 V for 70 min [20,21].

2.5. Fabrication of multi-functional DNA 3WJ/pRhNPs heterolayer

The Au electrode, which had 10 μm of gap between the working electrode and the counter electrode, was designed and fabricated by the conventional fabrication method (Fig. 2a) [20]. An electrode was composed of seven electrodes, resulting in seven times the measurement conducted with one electrode (Fig. 2b). The Au electrodes were washed by sonication with 99.5 % acetone for 5 min. Next, the electrodes were rinsed in ethyl alcohol, followed by deionized water, and dried under the N_2 gas stream. The Au surface of the electrodes was incubated with 10 mM cysteamine solution for self-assembled monolayer (SAM) formation. After incubation for 1 h, the pRhNPs were reacted with the modified electrodes for 2 h. Subsequently, 5 μl of 5 μM DNA 3WJ was dropped onto the pRhNPs-modified surface of the electrodes. The same amount of $AgNO_3$ solution was also added to surface and the reaction was allowed to proceed for 2 h. The entire procedure was carried out at room temperature.

2.6. Surface morphology analysis of pRhNPs-modified Au electrode

The surface of the pRhNPs-modified Au electrode was investigated by field effect scanning electron microscopy (FE-SEM) (Carl Zeiss, Germany). A Nanoscope IV/Multi-mode (Digital Instruments, USA) was used to measure the tapping-mode atomic force microscopy (AFM) by utilizing n-type doped Si Phosphorous tips (Bruker, USA). The resonance peaks in the frequency response were about 230–305 kHz and the spring constant of the cantilever was 20–80 N/m. The image size was 1.00 μm × 1.00 μm. The surface of the bare Au electrode was also measured for comparison.

2.7. Electrochemical measurement

After immobilization of the DNA 3WJ structure, the electrodes were allowed to react with the T4 solution overnight at 4 °C. The T4 aptamer sequence of 3 W J-a was bound to T4. The solution chamber was made up of PDMS and used as the working chamber on the Au electrode for electrochemical analysis (Fig. 2c) [22]. CV and EIS were performed using a VersaSTAT 3 Potentiostat (Princeton Applied Research, USA). CV was carried out under the potential range from 0.6 V to −0.1 V at 50 mV/s, and EIS parameters were as follows: frequency range from 100 kHz to 1 Hz under the DC potential of 0.37 V. For analysis, 5 mM $[Fe(CN)_6]^{3-/4-}$ redox repair (1:1 M ratio) in 10 mM HEPES (pH 7.03) containing 1 M KCl was used as the electrolyte. The Ag/AgCl reference electrode (CH Instruments, USA) was chosen as the reference electrode, which was used by dipping in solution. The probe tips made of copper were fabricated to contact with the counter electrode and working electrode parts of the electrode [23]. The edge of the tips was connected to the surface of the electrode (Fig. 2d).

3. Results and discussion

3.1. T4 DNA aptamer feasibility evaluation

Prior to fabricating the biosensor, it was necessary to confirm the binding ability of the T4 DNA aptamer to T4. ELAAs were performed to demonstrate the ability of the T4 DNA aptamer to bind T4. T4 was physically adsorbed to a 96-well plate. The target T4 and the corresponding aptamer bound to each other. Biotin-streptavidin binding was generated by streptavidin-Cy3 and biotin-tagging of the aptamer at the 5` end. Because the unbound residues fell off during the washing process between each step, a Cy3-coated 96-well plate was finally obtained. The biotin-tagged control DNA did not bind to T4, and was rinsed out during the washing steps. Hence, the results of the test using the control DNA showed relatively lower fluorescence intensity of Cy3 than that of the T4 DNA aptamer (Fig. 3a).

3.2. Binding assay with artificial and clinical samples of T4

The amino group of T4 allows for binding to CNBr-activated sepharose [17]. T4-sepharose was reacted with the biotinylated T4 DNA aptamer and streptavidin-Cy3 in turn. A complex containing sepharose, T4, T4 DNA aptamer, and Cy3 was consequently formed by the reaction of the T4 DNA aptamer and biotin-streptavidin. The recovery of sepharose-DNA-Cy3 complex was obtained following filtration by centrifugation. Fig. 3b shows the results of the tests using the T4 DNA aptamer and control DNA. The test results confirmed that the fluorescence intensity of the T4 DNA aptamer was higher than that of the control DNA. Analysis of clinical T4 samples was also performed using the same method (Fig. 3c). Similar to the artificial T4 samples, higher fluorescence intensity was observed for the T4 DNA aptamer than that for the control DNA. The error bars in Fig. 3c were larger compared to others, because the clinical samples were derived from plasma and

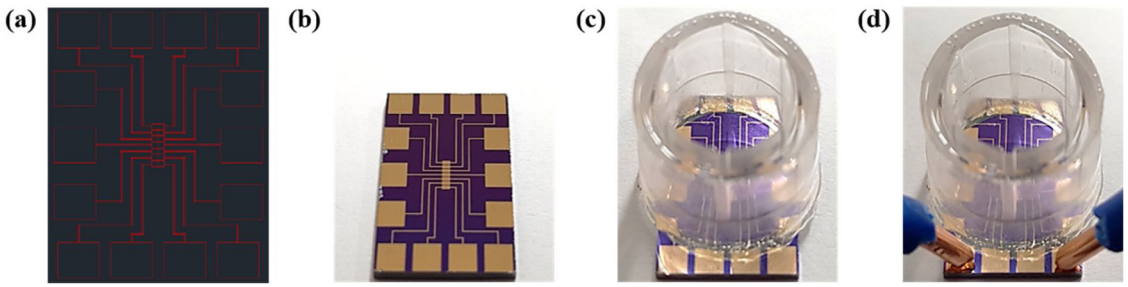

Fig. 2. (a) CAD image of the Au electrode, (b) Real picture of the Au electrode (10 mm × 15 mm), (c) Real picture of Au electrode with working chamber made by PDMS, (d) Real picture of Au electrode connected with probe tip.

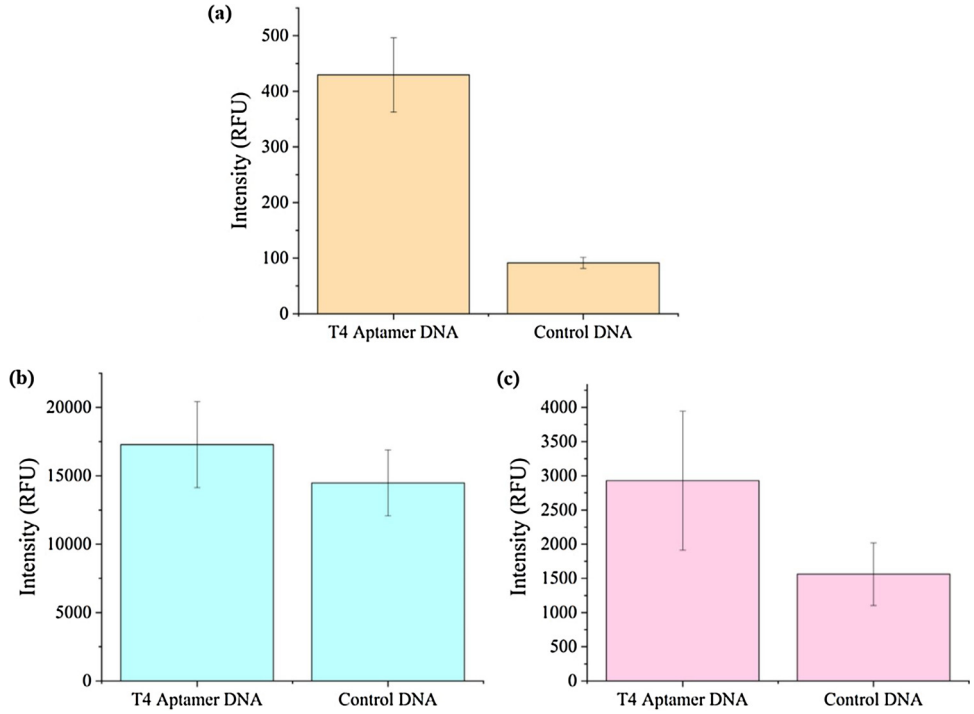

Fig. 3. Comparison of fluorescence intensity between T4 DNA aptamer and control DNA of the verification procedure: (a) by ELAA with artificial T4 samples, (b) by filtration with artificial T4 samples, (c) by filtration with clinical T4 samples (error bars: standard deviation).

contained several elements such as proteins and ions present in the human body. Based on the combined results, the binding of the T4 DNA aptamer and T4 was confirmed in both artificial and clinical T4 samples.

3.3. Confirmation of multi-functional DNA assembly

A multi-functional DNA bioprobe was thus designed using the T4 aptamer DNA that was confirmed to bind to the target, T4. 3WJ-a consisted of the T4 aptamer DNA sequence, which enabled the detection of T4. Four complementary C-C mismatched sequences were designed in 3WJ-b and 3WJ-c. Subsequently, silver ions were intercalated between the C-C mismatches to report the electrochemical signal. Additionally, the terminal of 3WJ-c was modified with a thiol for immobilization to the Au electrode. Fig. 4a shows the 2D structure of the DNA 3WJ structure with 3WJ-a, 3WJ-b, and 3WJ-c annealed in equimolar ratio. Assembly of the DNA 3WJ structure was confirmed using a 8% native TBM-PAGE (Fig. 4b). Lanes 2, 3 and 4 correspond to single-stranded DNAs of 3WJ-a, 3WJ-b, and 3WJ-c, respectively. The band present in lane 5 indicates a well-formed DNA 3WJ structure.

3.4. Investigation of pRhNPs-modified Au electrode

The surface of the pRhNPs-immobilized Au electrode was analyzed using FE-SEM and AFM. Fig. 5a and b showed the FE-SEM results (100 nm scale and 1 μm scale, respectively) for the pRhNPs-modified Au electrode, which confirmed that the pRhNPs were well immobilized. Fig. 5c and d displays the AFM image of the bare Au electrode and the fabricated pRhNPs-modified Au electrode, respectively. The horizontal size of pRhNPs was found to be around 80–250 nm. In addition, the surface roughness and vertical distance analysis were investigated. The roughness average (Ra), RMS roughness (Rq), maximum height (Rmax)

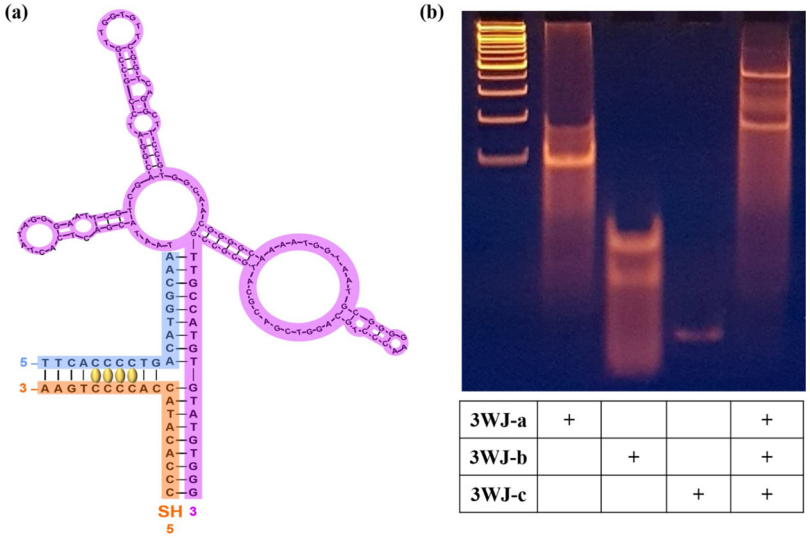

Fig. 4. (a) Schematic image of expected multi-functional DNA 3WJ structure from 3WJ-a of T4 aptamer for detection (purple line), 3WJ-b for signal reporter (blue line) and thiol modified 3WJ-c for immobilization (orange line) and intercalated silver ions (yellow circles), (b) TBM PAGE gel image of 3WJ-a, 3WJ-b, 3WJ-c and T4 DNA 3WJ structure. 100 bp DNA ladder was used.

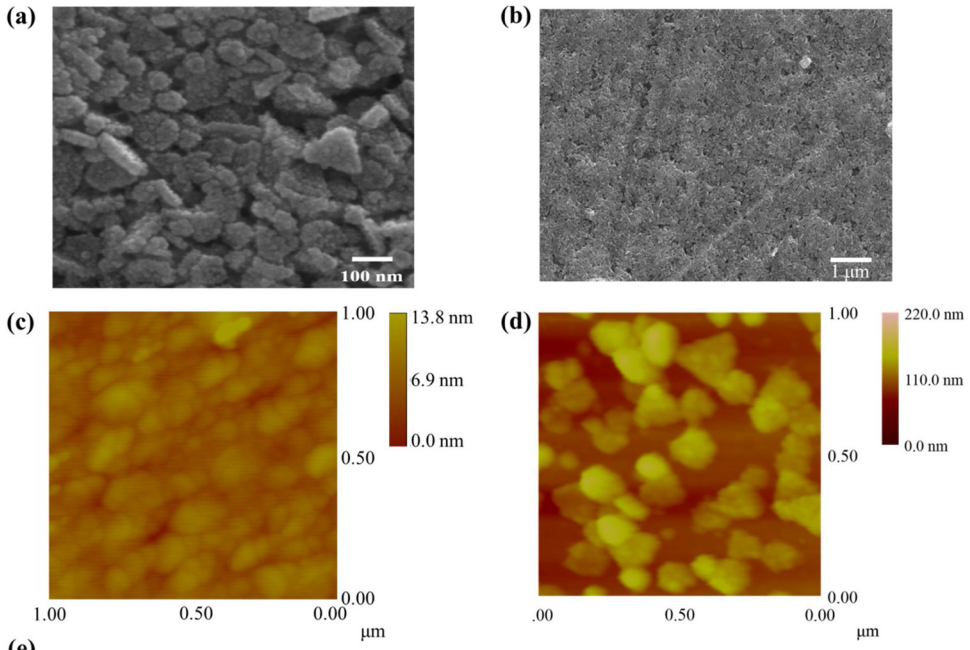

(e)

	Bare Au	Rhodium Nanoplate
Roughness Average (Ra) (nm)	0.485 ± 0.166	26.167 ± 8.699
RMS Roughness (Rq) (nm)	0.643 ± 0.222	29.519 ± 7.559
Maximum Height (Rmax) (nm)	2.621 ± 0.793	69.771 ± 14.249
Vertical Distance (nm)	1.187 ± 0.558	84.156 ± 4.814

Fig. 5. (a) Surface morphology of pRhNPs self-assembled Au electrode by FE-SEM, (100 nm scale) (b) Surface morphology of pRhNPs self-assembled Au electrode by FE-SEM, (1 μm scale) (c) Surface morphology of Au electrode by AFM, (d) Surface morphology of pRhNPs self-assembled Au electrode by AFM, (e) Surface roughness and vertical distance analysis of pRhNPs self-assembled Au electrode.

and vertical distance (VD) were 26.167 ± 8.699 nm, 29.519 ± 7.559 nm, 69.771 ± 14.249 nm and 84.156 ± 4.814 nm (Fig. 5e), respectively. Compared to Au substrate, the pRhNP showed the different morphology and surface roughness values. The surface morphology was similar to previous study [15]. Based on the result, the pRhNP was immobilized well on Au substrate for biosensor experiment.

3.5. Electrochemical response of T4 detection

Signal amplification was induced by using pRhNPs at the immobilization step. After anchoring the multi-functional DNA 3WJ structure, target T4 was reacted with the DNA 3 W J probe. The electrochemical response was measured by CV and EIS methods, which were performed with a three-electrode system. CV was performed at potential ranging from 0.6 V to −0.1 V at a scan rate of 50 mV/s in 5 mM $[Fe(CN)_6]^{3-/4-}$ solution in 10 mM HEPES (pH 7.03) containing 1 M KCl. Fig. 6a shows the cyclic voltammogram of each immobilization step. The pRhNPs-modified electrode had peak currents (I_p) similar to those of the bare Au electrode. In contrast, the I_p values of the DNA3WJ/pRhNPs/Au and T4/DNA3WJ/pRhNPs/Au electrodes decreased. The peak-to-peak separation of the redox potential peaks (ΔE_p) of the bare Au, pRhNPs/Au, DNA3WJ/pRhNPs/Au, and T4/DNA3WJ/pRhNPs/Au electrodes was 85.26, 91.78, 112.02, and 133.23 mV, respectively. Fig. 6b shows the EIS spectra performed within the frequency range of 100 kHz to 1 Hz at the DC potential of 0.37 V in the same solution as that used for CV. The EIS spectrum was analyzed using Randles equivalent circuit, where "R_s" is the solution-phase resistance, "C_{dl}" is the double-layer capacitance, "R_{ct}" is the charge-transfer resistance, and "Z_w" is the Warburg impedance (inset of Figs. 6b, 7 a, c ande). The R_{ct} values of the bare Au, pRhNPs/Au, and DNA3WJ/pRhNPs/Au electrodes were 1125.76, 1294.2, and 1759.95 Ω, respectively. A definite increase in R_{ct} was observed following DNA 3WJ immobilization. DNA is negatively charged with anionic phosphates. The redox couple of $[Fe(CN)_6]^{3-/4-}$ was disturbed by the introduction of the bioprobe-formed DNA. Following the reaction of T4 and DNA 3WJ on the electrode, the R_{ct} increased markedly to 4654.20 Ω. This phenomenon was attributed to the effect of the interfering electron transfer by the formation of the target-probe complex on the surface of

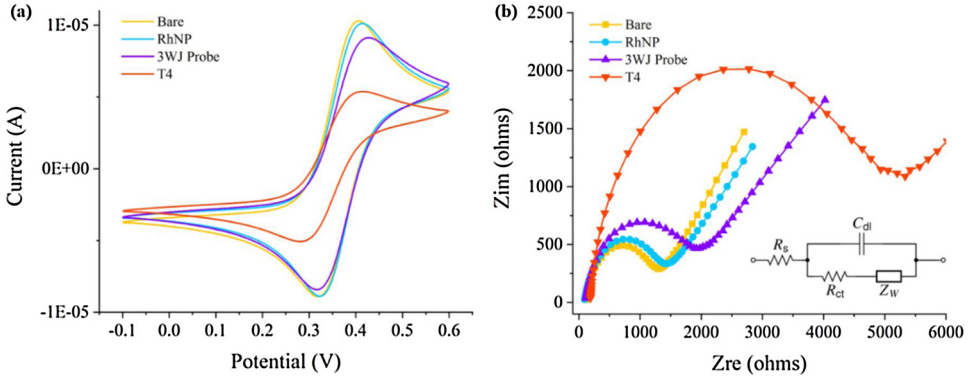

Fig. 6. (a) Cyclic voltammogram of different modified electrode with T4 (100 pM), DNA 3WJ (5 μM) and pRhNPs in 5 mM $[Fe(CN)_6]^{3-/4-}$ solution in 10 mM HEPES (pH 7.03) containing 1 M KCl on scan rate 50 mV. (b) Impedance spectra of different modified electrode with T4 (100 pM), DNA 3WJ (5 μM) and pRhNPs in 5 mM $[Fe(CN)_6]^{3-/4-}$ solution in 10 mM HEPES (pH 7.03) containing 1 M KCl. The frequency range was from 100 kHz to 1 Hz at the potential 0.37 V.

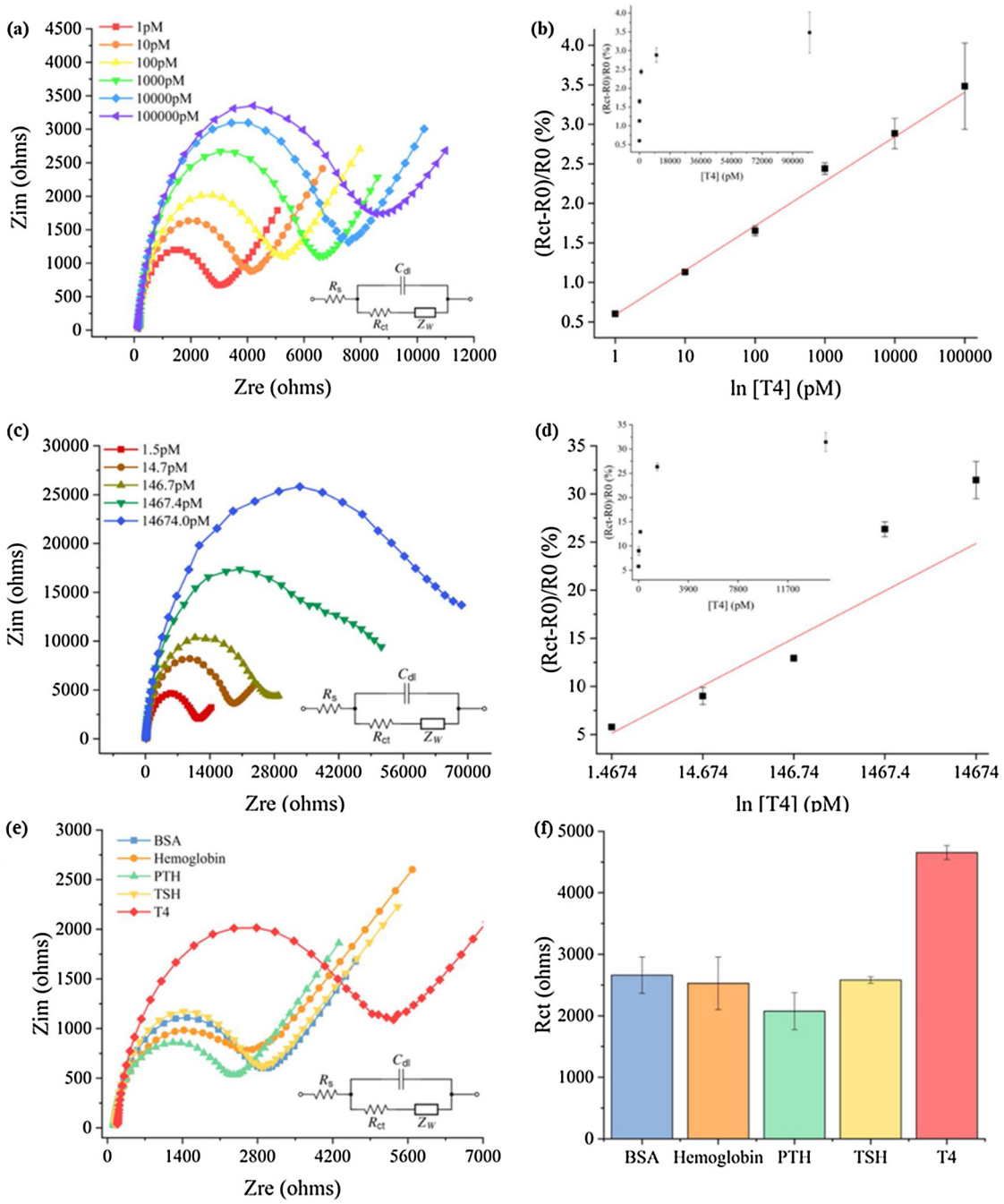

Fig. 7. (a) Impedance spectra of in different concentrations of T4 (artificial), (b) Calibration curve of in different concentrations of T4 (artificial); linear range from 100 nM to 1 pM. (c) Impedance spectra of in different concentrations of T4 (clinical), (d) Calibration curve of in different concentrations of T4 (clinical); linear range from 14.7 nM to 1.5 pM. (e) Impedance spectra of proposed biosenor with the various targets (100 pM) including BSA (blue line), hemoglobin (orange line), PTH (green line), TSH (yellow line) and T4 (red line), (f) Change in charge-transfer resistance based on selectivity (error bars: standard deviation).

the electrode. These results confirmed that the introduced system was able to detect T4.

3.6. Sensor performance

EIS response was obtained at different concentrations of T4, which can be applied for the rapid measurement of a number of samples with lower damage to the samples compared to CV. A 99 % confidence interval was established to estimate the data. The test was performed by serial dilutions in the concentration range from 100 nM to 1 pM (Fig. 7a). The diameter of the semicircle and R_{ct} values increased gradually as the T4 concentration increased. Fig. 7b shows the relationship between relative charge-transfer resistance $(R_{ct} - R_0)/R_0$ and T4 concentration by linear fitting [24,25] and regressed equation $(R_{ct} - R_0)/R_0 = 0.2537\ln[T4] + 0.5717$. The correlation coefficient (R^2) value was 0.9961. The limit of detection was calculated to be 10.33 pM based on the 3(SD/m) method, where "SD" is the standard deviation of the response and "m" is the slope of the linear calibration curve. Moreover, the test was further validated using clinical T4 samples from human plasma. The samples were measured by serial dilution in the concentration range from 14.7 nM to 1.5 pM (Fig. 7c). Expressed by equation $(R_{ct} - R_0)/R_0 = 2.1403\ln[T4] + 4.3116$, $R^2 = 0.8549$ was observed (Fig. 7d). The R^2 values of the clinical T4 samples were lower compared with those of the artificial T4 samples. The LOD was found to

Table 1
Comparison of the fabricated biosensor with other electrochemical sensors for T4.

No.	Receptor Materials	Detection Method	Detection Limit	Labeling	References
1	Antibody	DPV	15 fg/mL	Cascade catalysis of cytochrome c and glucose oxidase	[26]
2	Polyvinylpyrrolidone in the presence of cetyltrimethyl ammonium bromide	CV	80 nM	Label-free	[27]
3	MWNT-DHP	DPV	5 ng/mL	Label-free	[28]
4	Antibody	CV (with capillary electrophoretic enzyme immunoassay)	3.8 nM	HRP reaction of TMB with H_2O_2	[29]
5	Antibody	EIS	1.5 ng/mL	Label-free	[30]
6	Screen printed carbon electrodes (SPCEs)	DPV	3 nM	Label-free	[31]
7	β-cyclodextrin	CV	1 nM	Label-free	[32]
8	SWNT-DHP in the presence of cetyltrimethyl ammonium bromide	LSV	20 nM	Label-free	[33]
9	Aptamer/Rhodium Nanoplate	EIS	10.33 pM (in buffer) 11.41 pM (in human serum)	Label-free	Present work

Table 2
Comparison of the fabricated biosensor with conventional method (RIA) for T4 detection.

Detection Method	Receptor Materials	Detection Time	Comments	References
Radioimmunoassay (RIA)	Antibody	< 12 h	It was first developed in 1965 and has been in use until recently, but with low sensitivity to low concentration level. Two-step assay is clinically more useful than one-step assay, but the steps are complex. The risk of using radioactive materials exists.	[34,35]
Electrochemical	Aptamer	~1 h	Use relatively inexpensive aptamer compared to antibody. Accurate and fast measurement possible with simple steps.	Present work

be 11.41 pM, which was calculated using the 3σ rule. The LOD result was compared to previous study in Table 1. Fig. 7e and f showed the selectivity test of the fabricated biosensor to detect T4 (red color) in the artificial samples. The proteins included albumin (blue color), hemoglobin (orange color), PTH (green color), and TSH (yellow color), which were used as controls in the EIS experiments for selectivity. Based on the combined results, the present biosensor could detect the T4 in clinical samples with high selectivity. The proposed biosensor was compared to conventional detection method of T4 in Table 2.

4. Conclusions

The novel electrochemical biosensor for T4 detection based on the multi-functional DNA 3 W J structure and pRhNPs was fabricated. The sensing performance was achieved through EIS the detection of T4 in samples at different concentration ranges prepared by serial dilution of the artificial and clinical T4 samples. The lower limits of detection were 10.33 pM and 11.41 pM, respectively. The biosensor system reported in this study was confirmed to be able to detect T4 in both artificial and clinical samples. Since this system uses a multi-functional probe having the functions of detection, signal reporting, and immobilization, T4 can be detected in a label-free manner. The first application of pRhNPs in the fabrication of electrochemical biosensors has confirmed new possibilities for use in electrochemistry in terms of elements. Those multi-functional bioprobe with nanoparticle can easily apply the various sensing system not only electrochemical type but also electrical type, spectroscopic type and others. The present work is expected to facilitate faster and more accurate T4 detection than the conventional detection method. The proposed biosensor system will be applied to other small molecule detections in the near future.

CRediT authorship contribution statement

T.L. and M.L. rolled to Conceptualization and Writing; S.P. rolled to Investigation and Methodology. G.I. and H.J. rolled to Data curation. J.K. and Y.L. rolled to validation. S.K. and C.P. rolled to Investigation.

Declaration of Competing Interest

The authors declare that they have no known competing financial interests or personal relationships that could have appeared to influence the work reported in this paper.

Acknowledgements

This research was supported by Basic Science Research Program through the National Research Foundation of Korea (NRF) funded by the Ministry of Education (2018R1D1A1B07049407) and by Korea Environment Industry&Technology Institute (KEITI) through the program for the management of aquatic ecosystem health, funded by Korea Ministry of Environment (MOE) (2020003030001) and by the Ministry of Trade, Industry, and Energy (Grant. 10062995).

References

[1] P.M. Yen, Physiological and molecular basis of thyroid hormone action, Physiol. Rev. 81 (2001) 1097–1142.
[2] G.C. Schussler, The thyroxine-binding proteins, Thyroid 10 (2000) 141–149.
[3] M.P. Hage, S.T. Azar, The link between thyroid function and depression, J. Thyroid Res. (2012) 590648.
[4] X.H. Wang, S. Wang, Sensors and biosensors for the determination of small molecule biological toxins, Sensors 8 (2008).
[5] M. Liss, B. Petersen, H. Wolf, E. Prohaska, An aptamer-based quartz crystal protein biosensor, Anal. Chem. 74 (2002) 4488–4495.
[6] M. Minunni, S. Tombelli, A. Gullotto, E. Luzi, M. Mascini, Development of biosensors with aptamers as bio-recognition element: the case of HIV-1 Tat protein, Biosens. Bioelectron. 20 (2004) 1149–1156.

[7] K. Ikebukuro, C. Kiyohara, K. Sode, Novel electrochemical biosensor system for protein using the aptamers in sandwich manner, Biosens. Bioelectron. 20 (2005) 2168–2172.
[8] J. Zheng, L. Lin, G. Cheng, A. Wang, X. Tan, P. He, Y. Fang, Study on an electrochemical biosensor for thrombin recognition based on aptamers and nano particles, Sci. China B Chem. 50 (2007) 351–357.
[9] S. Atwell, E. Meggers, G. Spraggon, P.G. Schultz, Structure of a copper-mediated base pair in DNA, J. Am. Chem. Soc. 123 (2001) 12364–12367.
[10] V.A. Bloomfield, D.M. Crothers, Nucleic Acids: Structures, Properties, and Functions, University Science Books, 2000.
[11] A. Ono, H. Torigoe, Y. Tanaka, I. Okamoto, Binding of metal ions by pyrimidine base pairs in DNA duplexes, Chem. Soc. Rev. 40 (2011) 5855–5866.
[12] A. Ono, S. Cao, H. Togashi, M. Tashiro, T. Fujimoto, T. Machinami, S. Oda, Y. Miyake, I. Okamotoa, Y. Tanaka, Specific interactions between silver(I) ions and cytosine–cytosine pairs in DNA duplexes, Chem. Commun. (2008) 4825–4827.
[13] Y. Miyake, H. Togashi, M. Tashiro, H. Yamaguchi, S. Oda, M. Kudo, Y. Tanaka, Y. Kondo, R. Sawa, T. Fujimoto, T. Machinami, A. Ono, Mercury^{II}-mediated formation of Thymine-Hg^{II}-thymine base pairs in DNA duplexes, J. Am. Chem. Soc. 128 (2006) 2172–2173.
[14] E. Meggers, P.L. Holland, W.B. Tolman, F.E. Romesberg, P.G. Schultz, A novel copper-mediated DNA base pair, J. Am. Chem. Soc. 122 (2000) 10714–10715.
[15] S. Kang, W. Shin, M.-H. Choi, M. Ahn, Y.-K. Kim, S. Kim, D.-H. Min, H. Jang, Morphology-controlled synthesis of rhodium nanoparticles for cancer phototherapy, ACS Nano 12 (2018) 6997–7008.
[16] N. Kawazoe, Y. Ito, M. Shirakawa, Y. Imanishi, In vitro selection of a DNA aptamer binding to thyroxine, Bull. Chem. Soc. Jpn. 71 (1998) 1699–1703.
[17] D. Lévesque, J.-D. Beaudoin, S. Roy, J.-P. Perreault, In vitro selection and characterization of RNA aptamers binding thyroxine hormone, Biochem. J. 403 (2007) 129–138.
[18] C.B. Anfinsen, P. Cutarecasas, H. Taniuchi, 3rd edition, P.D. Boyer (Ed.), The Enzymes, 4 Academic Press, 1971, pp. 177–204.
[19] M. Mohammadniaei, J. Yoon, T. Lee, B.G. Bharate, J. Jo, D. Lee, J.-W. Choi, Electrochemical biosensor composed of silver ion-mediated dsDNA on Au-encapsulated Bi_2Se_3 nanoparticles for H_2O_2 detection, Small 14 (2018) 1703970.
[20] T. Lee, S.Y. Park, H. Jang, G.-H. Kim, Y. Lee, C. Park, M. Mohammadniaei, M.-H. Lee, J. Min, Fabrication of electrochemical biosensor consisted of multi-functional DNA structure/porous au nanoparticle for avian influenza virus (H5N1) in chicken serum, Mater. Sci. Eng. C 99 (2019) 511–519.
[21] T. Lee, M. Mohammadniaei, H. Zhang, J. Yoon, H.K. Choi, S. Guo, P. Guo, J.-W. Choi, MicroRNA detection: single functionalized pRNA/gold nanoparticle for ultrasensitive MicroRNA detection using electrochemical surface-enhanced Raman spectroscopy, Adv. Sci. 7 (2020) 2070012.
[22] T. Lee, Y. Lee, S.Y. Park, K. Hong, Y. Kim, C. Park, Y.-H. Chung, M.-H. Lee, J. Min, Fabrication of electrochemical biosensor composed of multi-functional DNA structure/Au nanospike on micro-gap/PCB system for detecting troponin I in human serum, Colloids Surf. B Biointerfaces 175 (2019) 343–350.
[23] R. Mazrouei, B. Huffman, M. Sumita, M. Shavezipur, Development of an impedance-based interdigitated biochemical sensor using a multiuser silicon process, J. Micromech. Microeng. 29 (2019) 075011.
[24] C.M. Li, W. Chen, X. Yang, C.Q. Sun, C. Gao, Z.X. Zheng, J. Sawyer, Impedance labelless detection-based polypyrrole protein biosensor, Front. Biosci. 10 (2005) 2518–2526.
[25] C.M. Li, C.Q. Sun, S. Song, V.E. Choong, G. Maracas, X.J. Zhang, Impedance labelless detection-based polypyrrole DNA biosensor, Front. Biosci. 10 (2005) 180–186.
[26] J. Han, Y. Zhuo, Y. Chai, Y. Yu, N. Liao, R. Yuan, Electrochemical immunoassay for thyroxine detection using cascade catalysis as signal amplified enhancer and multi-functionalized magnetic graphene sphere as signal tag, Anal. Chim. Acta 790 (2013) 24–30.
[27] Q. He, X. Dang, C. Hu, S. Hu, The effect of cetyltrimethyl ammonium bromide on the electrochemical determination of thyroxine, Colloids Surf. B Biointerfaces 35 (2004) 93–98.
[28] K. Wu, X. Ji, J. Fei, S. Hu, The fabrication of a carbon nanotube film on a glassy carbon electrode and its application to determining thyroxine, Nanotechnology 15 (2004) 287–291.
[29] Z. He, W. Jin, Capillary electrophoretic enzyme immunoassay with electrochemical detection for thyroxine, Anal. Biochem. 313 (2003) 34–40.
[30] R.A.S. Couto, L.M. Goncalves, M.S. G´oes, C.M.P. Rodrigues, M.B. Quinaz, J.A. Rodrigues, SAM-based immunosensor for the analysis of thyroxine (T4), J. Electrochem. Soc. 164 (2017) B103–B106.
[31] A. Das, M.V. Sangaranarayanan, Electroanalytical sensor based on unmodified screen-printed carbon electrode for the determination of levo-thyroxine, Electroanalysis 27 (2015) 360–367.
[32] J. Muñoz, M. Riba-Moliner, L.J. Brennan, Y.K. Gun'ko, F. Céspedes, A. González-Campo, M. Baeza, Amperometric thyroxine sensor using a nanocomposite based on graphene modified with gold nanoparticles carrying a thiolated β-cyclodextrin, Microchim. Acta 183 (2016) 1579–1589.
[33] F. Wang, J. Fei, S. Hu, The influence of cetyltrimethyl ammonium bromide on electrochemical properties of thyroxine reduction at carbon nanotubes modified electrode, Colloids Surf. B Biointerfaces 39 (2004) 95–101.
[34] S.W. Jung, S.Y. Chang, J.J. Cho, Prevalence of abnormal thyroid function test and significance of TSH in health examination, Korean J. Fam. Med. 14 (1993) 752–759.
[35] R. Gnanasekar, U.H. Nagvekar, N. Sivaprasad, Development and validation of a two-step free thyroxine radioimmunoassay based on antibody coated tubes, J. Liq. Chromatogr. Relat. Technol. 33 (2010) 1576–1586.